Wall-Selective Probing of Double-Walled Carbon Nanotubes Using Covalent Functionalization

Delphine Bouilly,[†] Janie Cabana,[‡] François Meunier,[†] Maxime Desjardins-Carrière,[¶] François Lapointe,[‡] Philippe Gagnon,[¶] Francis L. Larouche,[†] Elyse Adam,[¶] Matthieu Paillet,[‡,∥] and Richard Martel[‡,§,*]

[†]Département de Physique and [‡]Département de Chimie, Université de Montréal, C.P. 6128 Succursale Centre-Ville, Montréal, Québec H3C 3J7, Canada, [¶]Département de Génie Physique, École Polytechnique de Montréal, C.P. 6079 Succursale Centre-Ville, Montréal, Québec H3C 3A7, Canada, and [§]Regroupement Québécois sur les Matériaux de Pointe (RQMP). [∥]Present address: Université Montpellier 2, Laboratoire des Colloïdes, Verres et Nanomatériaux (UMR CNRS 5587), 34095 Montpellier, France.

ABSTRACT Double-walled carbon nanotubes (DWNTs) present an original coaxial geometry in which the inner wall is naturally protected from the environment by the outer wall. Covalent functionalization is introduced here as an effective approach to investigate DWNT devices. Performed using an aryldiazonium salt, the functionalization is reversible upon thermal annealing and occurs strictly at the surface of the outer wall, leaving the inner wall essentially unaltered by the chemical bonding. Measurements on functionalized DWNT transistors show that the electrical current is carried by the inner wall and provide unambiguous identification of the metallic or semiconducting character of both walls. New insights about current saturation at high bias in DWNTs are also presented as an illustration of new experiments unlocked by the method. The wall-selectivity of the functionalization not only enables selective optical and electrical probing of the DWNTs, but it also paves the way to designing novel electronic devices in which the inner wall is used for electrical transport while the outer wall chemically interacts with the environment.

KEYWORDS: double-walled carbon nanotubes · covalent functionalization · field-effect transistors · wall properties identification · reversibility

Double-wall carbon nanotubes (DWNTs) are part of the nanotube family that present intriguing properties, such as unidimensional electronic bands and an excellent ability to transport electrical current.[1] They are the simplest form of multiwalled carbon nanotubes (MWNTs), which makes them ideal objects to shed light on fundamental questions related to interwall couplings,[2−4] repartition of electrical current,[2,5−8] and energy or charge transfer processes between walls.[9,10] Their coaxial geometry also offers new opportunities because the inner wall is contained in a protected environment[11] while the outer wall can be exploited for self-assembling or sensing purposes. Addressing systematically these premises demands the ability to identify the electrical nature of both walls and also to probe each wall selectively. Among the existing characterization techniques, transmission electron microscopy (TEM) and resonant Raman spectroscopy are the most powerful to identify single DWNTs. First, TEM allows identification of the chirality of each wall of an individual DWNT, either by electron diffraction[12,13] or high-resolution imaging.[14] However, exposure to the electron beam is considerably destructive for the samples. Moreover, combining sample manipulation for TEM with transport techniques is challenging.[15,16] Second, resonant Raman spectroscopy allows researchers to selectively probe and characterize each wall of an individual DWNT,[17,18] but it requires the use of many laser lines or tunable lasers in order to meet the resonant excitation energy of each wall. Third, density gradient ultracentrifugation of DWNTs in surfactants allows sorting by outer wall electronic type, but the inner walls still exhibit a mixture of properties.[19] Thus, all of these techniques are either partial or require advanced experimental setups that are not readily available in most laboratories. Yet, none of these methods is well suited to investigate selectively the electrical properties of each wall.

Here, we introduce the use of covalent functionalization with aryldiazonium salts in order to study electronic phenomena occurring in DWNTs. Our strategy takes advantage of the coaxial geometry of DWNTs to chemically modify the outer wall while keeping the inner wall unaffected. By measuring the properties of pristine, functionalized, and defunctionalized DWNTs, we are able to demonstrate selective probing of the nanotube walls. This methodology has many advantages: it is simple, inexpensive, sensitive to any nanotube chirality, and mostly reversible. Using this method, we demonstrate that both the inner and outer

* Address correspondence to r.martel@umontreal.ca.

Received for review March 17, 2011 and accepted May 19, 2011.

Published online May 19, 2011
10.1021/nn201024u

walls can transport electrical current with similar intensities at finite bias, and that their electrical character, metallic or semiconducting, can be independently identified. Moreover, we show that field-effect transistors made of functionalized DWNT channels can operate with transport characteristics similar to those of single-walled carbon nanotube (SWNT) devices. Finally we apply this method to study the phenomenon of current saturation at high bias in DWNTs. We show that the inner wall exhibits current saturation when inside the functionalized outer wall, leading to new insights on the underlying carrier velocity saturation mechanism.

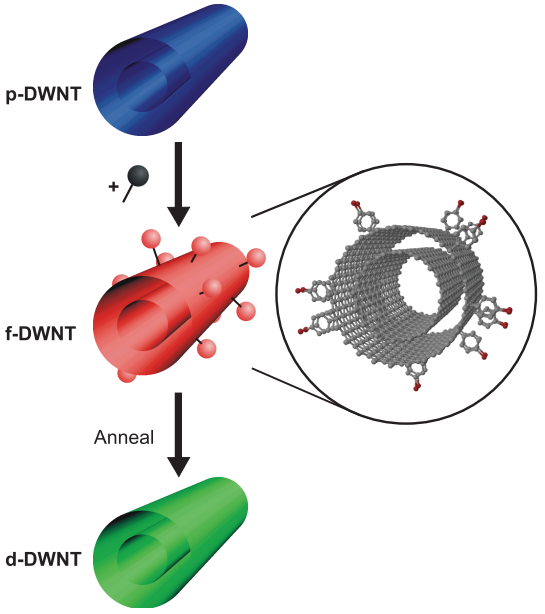

Figure 1. Sketch of the methodology based on covalent functionalization. A pristine DWNT (p-DWNT) is shown on top in blue. Covalent addition of chemical groups forms a functionalized DWNT (f-DWNT), illustrated in the middle in red. Thermal annealing leads to a defunctionalized DWNT (d-DWNT) on bottom in green. The color code for the three states is kept throughout this paper. Enlarged section: atomistic representation of a DWNT covalently functionalized using a 4-bromophenyldiazonium reaction.

RESULTS AND DISCUSSION

Methodology. Pristine DWNTs (p-DWNTs) were synthesized by chemical vapor deposition[20] and are studied here either in thin film networks or individually as field-effect transistor devices. In both cases, the procedure schematized in Figure 1 was followed. First, functionalized DWNTs (f-DWNTs) are formed by the covalent bonding of chemical groups on the sidewall. Second, the f-DWNTs are annealed, forming thermally defunctionalized DWNTs (d-DWNTs). In this work, a diazonium salt reaction is used, leading to grafting of 4-bromophenyl groups,[21] as illustrated in the enlarged part of Figure 1. This functionalization was chosen because it is known to drastically decrease the conductivity[22] and the optical response[23] of SWNTs, and also to be mostly reversible upon annealing at 500 °C.[24]

Wall-Selectivity of the Functionalization. It is first relevant to confirm that the functionalization of DWNTs occurs only on the outer wall and is mostly reversible. In order to do so, absorption spectra of a DWNT thin film are acquired in pristine, functionalized and defunctionalized states, as presented in Figure 2a. Data from the pristine state shows a set of peaks in the optical range of 1000−2500 nm. The large peak centered around 2000 nm is associated to the first optical transition of

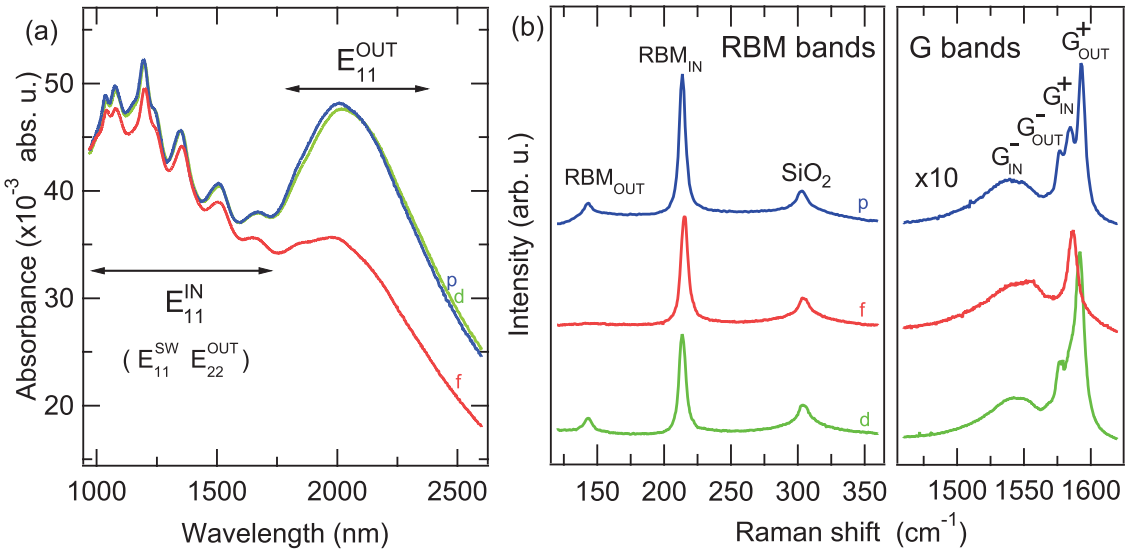

Figure 2. (a) Absorption spectra of a DWNT thin film in pristine (p-blue), functionalized (f-red), and defunctionalized (d-green) states. Regions of the spectra are assigned either to the first optical transition of the outer (E_{11}^{OUT}) or of the inner (E_{11}^{IN}) walls of the DWNTs. Minor contributions of the first optical transition of SWNTs (E_{11}^{SW}) and of the second optical transition of the outer wall of DWNTs (E_{22}^{OUT}) are also indicated. (b) Raman spectra of an individual DWNT in the pristine (p-blue), functionalized (f-red), and defunctionalized (d-green) states, in the range of RBM and G modes. Spectra are vertically shifted for clarity. Peaks are assigned to the outer (OUT) or the inner (IN) wall of the DWNT, or to the SiO_2 substrate.

the semiconducting outer walls (E_{11}^{OUT}).[25] The other peaks in the range of 1000−1750 nm can be mostly related to the first optical transition of semiconducting inner walls (E_{11}^{IN}), but also to the first optical transition of residual semiconducting SWNTs (E_{11}^{SW}) and to the second optical transition of semiconducting DWNT outer walls (E_{22}^{OUT}).[25] Those last two contributions are known to be less intense than the first one, due to the smaller concentration of SWNTs (18% in pristine sample)[20] and because the response of the second optical transition is lower than the first one. After functionalization of the film, the E_{11}^{OUT} peak greatly diminishes while the rest of the spectrum is much less affected. Considering that the loss of optical response is attributed to the grafting of phenyl groups,[23] the functionalization must occur only on the outer wall of DWNTs. The inner walls are therefore unaffected by the reaction, in agreement with previous experiments performing fluorination or oxidation of DWNTs.[25−27] The small decrease of intensity observed for the other peaks can be explained by the minor contributions of E_{11}^{SW} and E_{22}^{OUT}, which are both expected to be affected by the functionalization. Moreover, the defunctionalized spectrum is superposed over the pristine one, therefore showing a good level of reversibility for this functionalization.

A similar trend is observed with individual DWNTs using resonant Raman spectroscopy. Figure 2b shows spectra taken at 633 nm in the radial breathing modes (RBM) and in the in-plane optical modes (G modes) regions of an individual DWNT in pristine, functionalized, and defunctionalized states. In the RBM region (100−300 cm^{-1}), the pristine spectrum shows two peaks. Since RBM frequency depends inversely on the diameter,[28] these are attributed to the inner wall (210 cm^{-1}) and the outer wall (145 cm^{-1}). The peak measured at 300 cm^{-1} is due to the SiO_2 substrate and is used for calibration purpose. Further details on the Raman analysis are provided in the Supporting Information. After functionalization, the RBM peak from the outer wall completely vanishes while the response of the inner wall is preserved, although a small upshift is noted in its frequency. All peaks are restored in the defunctionalized state, in particular the RBM peak from the outer wall has regained most of its initial height. In the G mode region (1500−1650 cm^{-1}), the pristine spectrum shows four peaks, the two highest are assigned to the G^+ components of each two walls and the two lowest to the G^- ones.[17,28,29] The G^- component frequency is known to decrease with decreasing diameter, and its line shape is strongly dependent on the metallic or semiconducting character of the nanotube.[28,29] The wide peak observed at 1540 cm^{-1} is thus attributed to a small metallic wall and the thin peak at 1575 cm^{-1} to a large semiconducting wall. After functionalization, the G^- component of the outer wall disappears along with one of the G^+ modes, leaving the two G modes of the inner wall intact. Again, the peaks from the outer wall reappear almost fully in the defunctionalized state. All of these optical measurements converge to demonstrate that functionalization attacks only the outer wall, killing its optical response in the process. Covalent functionalization can therefore be used to isolate the signal from the inner wall. Moreover, the good reversibility of the reaction allows one to isolate and compare the properties of each wall without losing at the end the pristine properties of the DWNT.

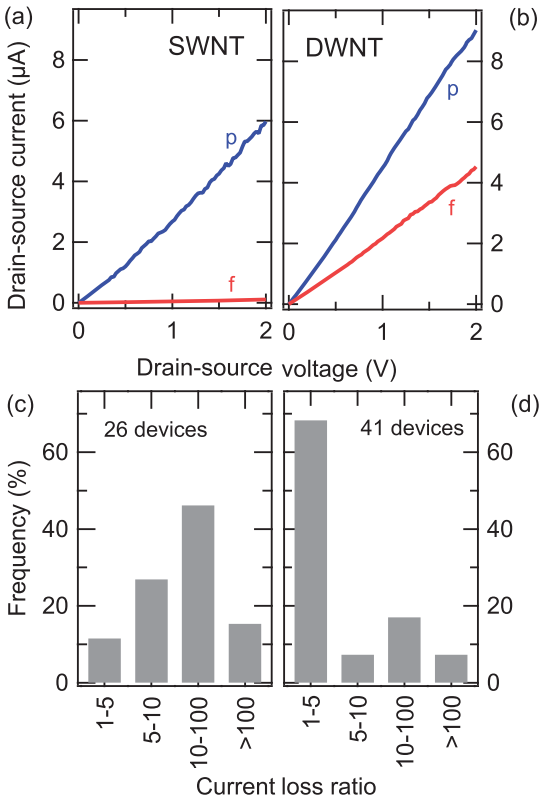

Figure 3. (a) Electrical current in an individual SWNT device as a function of drain voltage, in pristine (p-blue) and functionalized (f-red) states. Gate voltage is −15 V. (b) Same as in panel a for a DWNT device. (c) Distribution of current loss ratios calculated for all 26 SWNT devices following covalent functionalization. (d) Same as panel c for all 41 DWNT devices.

Electrical Transport of Both Walls. The same methodology is then used to study electrical properties of individual DWNTs in field-effect transistor devices. For means of comparison, the study is also performed on individual SWNTs. Diameter measurements acquired using atomic force microscopy are used to reject large bundles, as well as residual SWNTs present in the DWNT samples. Devices showing very small currents in the pristine state are also removed from this study. Electrical measurements are performed on 26 individual SWNT devices and 41 individual DWNT devices. In these measurements, gate voltage is fixed at −15 V in order to allow conduction in the semiconducting channels as well as in the metallic ones. Figure 3a presents electrical current as a function of

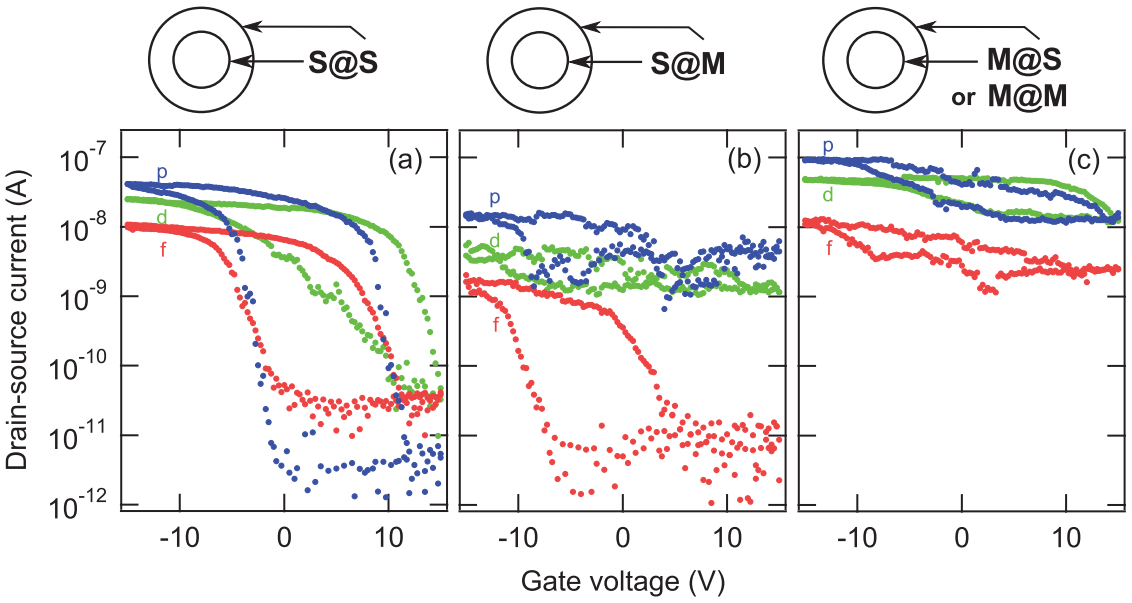

Figure 4. Electrical current in individual DWNT devices in the pristine (p-blue), functionalized (f-red), and defunctionalized (d-green) states as a function of gate voltage. Drain−source voltage is 10 mV. Three electrical signatures are distinguishable and assigned to the following electrical combinations: (a) S@S, (b) S@M, and (c) M@S/M@M. See text for more details on this assignation.

drain−source voltage for a typical SWNT device in pristine and functionalized states. The pristine curve shows current increasing to several microamps. Functionalization of the SWNT device has a dramatic effect, with a current reduction of more than an order of magnitude, which is consistent with past studies.[22,24,30] Theoretical work has ascribed such a current loss to an increase of backscattering due to quasibound states induced by defects.[31] In comparison, the same measurement is presented in Figure 3b for a typical DWNT device. In the pristine state, the current is higher but comparable to the one presented for the SWNT. The effect of functionalization of DWNTs is however quite different: the current is reduced by approximately a factor of 2, which is considerably less than in the case of SWNT, and the residual current is comparable to the current carried by the pristine SWNT.

Statistical analysis of all the SWNT and DWNT measurements is performed by calculating the current loss ratio, that is, the pristine current divided by the functionalized current at 1 V bias. Figure 3 panels (c) and (d) present the distribution of current loss ratios obtained respectively for SWNT and DWNT devices. Dispersion in both distributions is due to heterogeneities of the nanotube properties and to the selectivity of the reaction. In the case of SWNT, functionalization is shown to cause a modal current loss of 1 to 2 orders of magnitude. The current loss is considerably smaller for the DWNT devices, with a ratio of only 1 to 5.

Considering that the functionalization decreases the SWNT conductivity by more than 1 order of magnitude, and that it occurs only on the outer wall of DWNTs (as demonstrated earlier with optical measurements), the residual conductivity of functionalized DWNTs can be safely attributed to the inner wall. This proves unambiguously that the inner wall can transport electrical current, which complements previous measurements on DWNT networks.[32] Moreover, the magnitude of the current loss in the case of a functionalized DWNT, by a factor between 1 and 5, suggests that the amount of current transported by both walls is similar. Our work thus allows for the first time the isolation of the electrical response of the inner wall of a DWNT and demonstrates that functionalized DWNT transistors can operate with a good level of current flowing through the inner wall.

Characterization of Electrical Combinations. Finally, electrical measurements as a function of gate voltage are explored for all the DWNT devices, in pristine, functionalized, and defunctionalized states, with a small source−drain voltage (10 mV). Three distinct electrical signatures are observed in those characteristics. The first one (Figure 4a) is easily recognizable by a strong modulation (*i.e.*, by several orders of magnitude) of the current upon variation of gate voltage, in pristine as well as functionalized and defunctionalized states. Considering that the current measured for a functionalized DWNT is due to the inner wall, such a modulation in this state indicates the presence of a semiconducting inner wall. Moreover, since the pristine and defunctionalized states also show strong modulation resulting from both the inner and outer walls, the outer wall must also be semiconducting. This signature is thus assigned to a combination of two semiconducting walls (S@S).

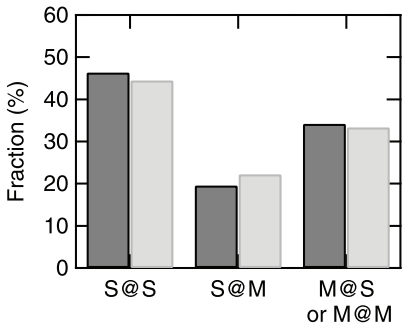

Figure 5. Distribution of all 41 DWNT devices in the three different electrical signatures. Black is for experimental measurements and gray is for the expected theoretical distribution ($^4/_9$ of S@S, $^2/_9$ of S@M, and $^3/_9$ of M@S+M@M).

The second signature (Figure 4b) also shows strong modulation in the functionalized state, but no modulation in the pristine and defunctionalized states. As for the latter case, the strong modulation in functionalized state identifies the inner wall as semiconducting. However, the absence of modulation observed in its pristine state requires the presence of a metallic outer wall. In this case, the constant current flowing in the metallic wall masks the modulation due to the inner wall in the logarithmic scale. This signature is thus assigned to a semiconducting core inside a metallic wall (S@M). This combination of properties is particularly interesting since this device can be switched from metallic to semiconducting character by a simple chemical reaction, and reverted to metallic character using annealing, as shown in the defunctionalized state.

The third and last signature (Figure 4c) shows no current modulation in any of the three states. The absence of modulation in the functionalized state indicates the presence of a metallic inner wall. However no conclusion can be extracted concerning the outer wall because the constant current contribution from the metallic inner wall masks the possible modulation of the outer wall. This signature can thus be assigned to either a metallic core inside a semiconducting wall (M@S) or a combination of two metallic walls (M@M).

To the extent of available laser lines, these assignations have been independently corroborated using resonant Raman spectroscopy (see Supporting Information). Moreover, the statistical distribution of electrical combinations follows what is theoretically expected. Since a random distribution of single-walled carbon nanotubes is composed of two-thirds of semiconducting and one-third of metallic species, combining two walls into forming a DWNT gives $^1/_9$ of M@M, $^2/_9$ of M@S, $^2/_9$ of S@M and $^4/_9$ of S@S. Figure 5 shows the distribution of the observed and predicted electrical distributions. Both are similar, which indicates first that the wall combinations indeed follow the random distribution of metallic and semiconducting species, and second that the classification proposed here based on electrical signature is appropriate. The process presented in this report is therefore an efficient way to identify the electrical combination of walls forming a DWNT. Moreover, the method is mostly reversible, since only a small current loss is observable in defunctionalized curves compared to pristine ones. This loss is consistent with previous experiments on SWNTs and attributed to a small accumulation of lattice defects following the defunctionalization process.[24] Nevertheless, the electrical signatures are clearly restored, as illustrated in Figure 4. Finally, the method is simple to use and has the great advantage of being effective with any chirality.

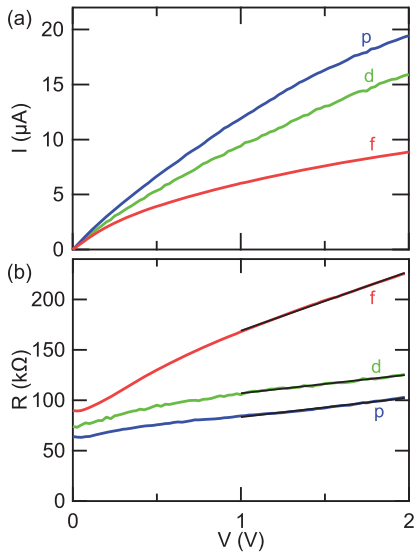

(c)

	I_0(μA)	R_0(kΩ)
p	52 ± 1	63.9 ± 0.4
f	17.0 ± 0.1	108.7 ± 0.4
d	54 ± 1	88.2 ± 0.5

Figure 6. Current saturation in an individual metallic DWNT device in ambient conditions. (a) Drain−source current observed in pristine (p-blue), functionalized (f-red), and defunctionalized (d-green) states as a function of drain−source voltage. Gate voltage is −15 V. (b) Experimental resistance for each three states as a function of drain−source voltage. Black lines are fits of eq 1 on the high bias data. (c) Values of I_0 and R_0, extracted from the fit for pristine (p), functionalized (f), and defunctionalized (d) states.

Case Study: Current Saturation at High Bias. The method introduced here can be used to gain new insights on electronic phenomena occurring in carbon nanotubes. For example, electrical current flowing in carbon nanotubes is known to undergo saturation when entering a high bias regime, both in SWNTs[33−35] and MWNTs.[7,36] This effect is generally ascribed to a saturation of the drift velocity of carriers due to backscattering by hot optical phonons, which is a mechanism activated only at high bias.[33,37] This phenomenon can be further explored in double-walled carbon nanotubes using the approach of covalent functionalization

described before. Figure 6a presents the electrical current flowing in an individual DWNT as a function of drain−source voltage, in pristine, functionalized, and defunctionalized states, with a gate voltage of −15 V. This DWNT was characterized as having a metallic inner wall (M@S or M@M) (see Supporting Information for detailed characterization) and presents excellent electrical properties, with low contact resistance and a clear current saturation at high bias in all three states of functionalization. In particular, the electrical response of the functionalized DWNT shows that current saturation occurs in the inner wall even when inside the functionalized outer wall.

Current saturation can be described using a simple two-variable model proposed by Z. Yao *et al.*,[33] in which the resistance R goes as

$$R = R_0 + V/I_0 \quad (1)$$

where V is the applied voltage, I_0 is the saturation current, and R_0 is the zero-bias resistance of the nanotube. The DWNT experimental resistance, calculated by dividing the voltage by the current for each data point in Figure 6a, is shown in Figure 6b for pristine, functionalized, and defunctionalized states. When drain−source voltage exceeds 1 V, the resistance shows a linear behavior, on which a regression of eq 1 is performed, leading to adjusted values of I_0 and R_0 for all three states (see table in Figure 6c). All zero-bias resistances R_0 are as low as several tens of kOhms, which is very good for an individual nanotube device. R_0 increases significantly between pristine and functionalized states, probably due to the wall-to-wall barrier for carrier injection. After defunctionalization, R_0 decreases but remains higher than in the pristine state. The I_0 behavior is different: saturation currents are roughly equivalent for the pristine and defunctionalized states, respectively 52 ± 1 μA and 54 ± 1 μA, and drop to 17.0 ± 0.1 μA in the functionalized state.

These measurements lead to original perspectives about the current saturation phenomenon. First, the increase of zero-bias resistance between pristine and defunctionalized states is consistent with previous experiments on the reversibility of the reaction, which reported small accumulations of defects.[24] The absence of I_0 variation is also expected considering that the origin of current saturation is related to phonon interaction rather than scattering on defects. Second, in functionalized state, the inner wall saturation current (17 μA) is close, although lower, to the 25 μA generally assumed for a SWNT in the literature.[33] Also, the maximum current of the whole DWNT is more than twice the current saturation of the inner wall, suggesting that the electrical properties in DWNTs are overall more complex than the sum of two equal contributions from each wall. These observations are compatible with the diameter dependent saturation behavior reported elsewhere[36] and suggest additional contributions to the phonon scattering mechanism presented by Z. Yao *et al.*[33] Last, the inner wall is observed to undergo current saturation without defunctionalizing the outer wall, a process that is known to take place at around 600 K.[38] This allows us to conclude that the whole nanotube is not significantly heated during saturation. Since the saturation mechanism is expected to generate an out-of-equilibrium population of optical phonons,[37] this new information is significant to the understanding of the thermalization path of these hot phonons in the nanotube lattice and environment. Overall, these measurements illustrate the uniqueness and capability of our approach for investigating complex transport phenomena in double-walled nanotubes.

CONCLUSION

The method introduced here provides wall-selective probing of DWNTs, thereby allowing a direct determination of the wall properties. Covalent functionalization is revealed as a powerful technique to explore fundamental electronic phenomena in DWNTs, such as interwall couplings, current repartition between walls or velocity saturation of carriers. This method is general and can be applied to other systems such as MWNTs and layered graphene devices. Moreover, beside the aryldiazonium salt reaction, the approach can be generalized to many other covalent functionalization schemes. Since our findings indicate that the inner wall is electrically active, functionalized DWNTs appear as a promising building block for assembling novel electronic devices with well-defined chemical functions.

EXPERIMENTAL DETAILS

Fabrication of DWNT Films. Catalyst-free pristine DWNTs were refluxed in a 10% v/v HNO_3 solution for 4 h followed by filtration. A subsequent reflux was done in ultrapure water (18.2 MΩ.cm) for 2 h, followed by filtration. The nanotubes were then dispersed in an aqueous solution of sodium cholate 1% w/v by sonicating in a bath. The dispersion was ultracentrifuged at 5000*g* (5400 rpm) for 1 h and the upper 80% supernatant was collected. Films were made by vacuum filtration of this solution and then transferred on a quartz substrate. The samples were annealed at 800 K for an *in situ* oxidation treatment and reheated at 1073 K in vacuum to ensure complete removal of surfactant and leftover residues from the deposition process. This last step also eliminated unintended doping by prior acidic and oxidation treatments. Finally, TEM images of the films were acquired to ensure the DWNT cleanness.

Fabrication of Individual SWNT and DWNT Field-Effect Transistors. All devices were fabricated using solution-based deposition of carbon nanotubes on a prepared surface followed by deposition of patterned metallic electrodes on top.[39] For SWNT devices, raw carbon nanotubes synthesized using a laser ablation method[40] were first purified by a reflux in nitric acid (10% by volume for 24 h) followed by a reflux in water for 2 h. Purified SWNTs were then suspended in dimethylformamide (DMF), and

the suspension was centrifugated and sonicated in a bath to decrease the concentration of SWNT bundles. For DWNT devices, nanotubes synthesized by chemical vapor deposition[20] were used after removal of catalyst using HCl, and dispersed in 1,2-dichloroethene (DCE) by sonication. The suspension was left for decantation for 2 weeks, and the supernatant was collected. In both cases, 100 nm SiO_2/n^+ Si wafers were used as a substrate. For SWNTs, the SiO_2 surface was functionalized using a piranha solution treatment followed by an aminosilane (APTS) vapor exposition, in order to have carbon nanotubes to adhere to the surface.[41] Note that a piranha solution reacts violently with organic materials and should be handled with extreme caution. For DWNTs, wafers were RCA cleaned. In each case, drops of the solution were deposited by spin-coating on the substrate, aligning in the process the nanotubes radially in direction of the liquid flow. Solution concentration and number of drops were adjusted so as to isolate nanotubes on the substrate. For SWNTs, additional drops of DCE were deposited by spin-coating in order to rinse and dry. For DWNTs, substrates were washed for 1 min in acetone by sonication at low power in order to remove amorphous carbon residues and larger bundles, and were subsequently rinsed in ethanol and dried in a N_2 stream. After deposition, electrodes were defined by optical lithography and deposited using e-beam evaporation of 0.5 nm Ti and 20 nm of Pd, followed by liftoff. Last, an annealing in vacuum at 550 °C was performed. Atomic force microscopy (AFM) imaging was systematically performed on all devices in order to ensure that only invidual carbon nanotube devices were used for the study. Note that small bundles of carbon nanotubes are difficult to distinguish from individual ones using AFM. Therefore, some of those small bundles may remain, which does not affect the conclusions since they are expected to be affected similarly by the functionalization process.

Covalent Functionalization Process. Ultrapure water was first deoxygenated and its pH was adjusted to ~9 using sodium hydroxide. Afterward, 4-bromobenzene diazonium tetrafluoroborate was dissolved to obtain a 2 mM solution. Such a high concentration of reactants was used in order to prevent any selectivity of the grafting reaction with wall chirality or diameter. The substrates were then immediately immersed in the mixture and allowed to react for 10 min at room temperature. The substrates were subsequently rinsed with ultrapure water and diethyl ether.

Defunctionalization Process. Annealing of the samples was performed in vacuum at 770 K at a pressure below 5×10^{-5} Torr. The temperature was maintained for 45 min, then cooled slowly to room temperature before breaking the vacuum.

Absorption Spectroscopy Experiments. Optical absorption spectra were acquired under rough vacuum with a Brüker Vertex 80v Fourier transform spectrometer equipped with a liquid nitrogen cooled MCT detector. A CaF_2 beamsplitter and a tungsten source were used, along with an aperture size of 0.5 mm, a resolution of 4 cm^{-1} and a scanning frequency of 20 kHz; 1024 scans were accumulated for each spectrum. The open beam was taken as the reference spectrum I_0, and sample spectra I were acquired at different spots on the slide, as defined by a 2 mm opening in front of the sample. Absorbance was then computed as $A = -\log(I/I_0)$. The spectrum from the quartz substrate was subtracted from the sample spectra to remove bands pertaining to the substrate. The final spectrum is the result of the averaging of seven different spots on the sample to attenuate the effect of film inhomogeneities.

Raman Spectroscopy Experiments. Raman measurements were performed on a high performance Raman spectroscopy setup[42] with fixed laser lines at 488, 532, 632.8, and 785 nm. The setup allowed horizontal displacements of the sample by 25-nm steps, and the laser spot size was between 500 and 800 nm. Measurements were performed on individual DWNT field-effect transistors (described above) with electrode separation of at least 1 μm. The sample position was adjusted so as to align the laser polarization parallel to the DWNT and to center the laser spot between the two electrodes. Spectra were acquired in the RBM region (~125 to ~800 cm^{-1}) and the D and G band regions (~1200 to ~1700 cm^{-1}) with a precision of ±1 cm^{-1}.

Electrical Transport Experiments. Transport measurements were performed with an ambient probe station using tungsten probes at room temperature. Current and voltage data were acquired using an Agilent B1500A semiconductor parameter analyzer.

Acknowledgment. The authors would like to thank E. Flahaut for providing the DWNTs and B. Simard for SWNTs. Valuable discussions with M. Côté and C. Silva are acknowledged. Financial support for this work is from the CRSNG Discovery and Canada Research Chair grants. D.B. acknowledges the receipt of a CRSNG Vanier CGS fellowship.

Supporting Information Available: Details on the assignation to S@S, S@M, M@S, and M@M. This material is available free of charge *via* the Internet at http://pubs.acs.org.

REFERENCES AND NOTES

1. Pfeiffer, R.; Pichler, T.; Kim, Y. A.; Kuzmany, H. In *Carbon Nanotubes: Advanced Topics in the Synthesis, Structure, Properties, and Applications*; Jorio, A., Dresselhaus, G., Dresselhaus, M. S., Eds.; Springer-Verlag: Berlin, 2008; Vol. 111, pp 495–530.
2. Charlier, J. C.; Blase, X.; Roche, S. Electronic and Transport Properties of Nanotubes. *Rev. Mod. Phys.* **2007**, *79*, 677–732.
3. Miyamoto, Y.; Saito, S.; Tomanek, D. Electronic Interwall Interactions and Charge Redistribution in Multiwall Nanotubes. *Phys. Rev. B* **2002**, *65*, 041402(R).
4. Song, W.; Ni, M.; Lu, J.; Gao, Z. X.; Nagase, S.; Yu, D. P.; Ye, H. Q.; Zhang, X. W. Electronic Structures of Semiconducting Double-Walled Carbon Nanotubes: Important Effect of Interlay Interaction. *Chem. Phys. Lett.* **2005**, *414*, 429–433.
5. Uryu, S.; Ando, T. Electronic Intertube Transfer in Double-Wall Carbon Nanotubes with Impurities: Tight-Binding Calculations. *Phys. Rev. B* **2007**, *76*, 155434.
6. Zolyomi, V.; Koltai, J.; Rusznyak, A.; Kuerti, J.; Gali, A.; Simon, F.; Kuzmany, H.; Szabados, A.; Surjan, P. R. Intershell Interaction in Double Walled Carbon Nanotubes: Charge Transfer and Orbital Mixing. *Phys. Rev. B* **2008**, *77*, 245403.
7. Collins, P. G.; Hersam, M.; Arnold, M.; Martel, R.; Avouris, P. Current Saturation and Electrical Breakdown in Multiwalled Carbon Nanotubes. *Phys. Rev. Lett.* **2001**, *86*, 3128–3131.
8. Bourlon, B.; Miko, C.; Forro, L.; Glattli, D. C.; Bachtold, A. Determination of the Intershell Conductance in Multiwalled Carbon Nanotubes. *Phys. Rev. Lett.* **2004**, *93*, 176806.
9. Green, A. A.; Hersam, M. C. Processing and Properties of Highly Enriched Double-Wall Carbon Nanotubes. *Nat. Nanotechnol.* **2009**, *4*, 64–70.
10. Tsyboulski, D. A.; Hou, Y.; Fakhri, N.; Ghosh, S.; Zhang, R.; Bachilo, S. M.; Pasquali, M.; Chen, L. W.; Liu, J.; Weisman, R. B. Do Inner Shells of Double-Walled Carbon Nanotubes Fluoresce? *Nano Lett* **2009**, *9*, 3282–3289.
11. Pfeiffer, R.; Kuzmany, H.; Kramberger, C.; Schaman, C.; Pichler, T.; Kataura, H.; Achiba, Y.; Kurti, J.; Zolyomi, V. Unusual High Degree of Unperturbed Environment in the Interior of Single-Wall Carbon Nanotubes. *Phys. Rev. Lett.* **2003**, *90*, 225501.
12. Kociak, M.; Suenaga, K.; Hirahara, K.; Saito, Y.; Nakahira, T.; Iijima, S. Linking Chiral Indices and Transport Properties of Double-Walled Carbon Nanotubes. *Phys. Rev. Lett.* **2002**, *89*, 155501.
13. Colomer, J. F.; Henrard, L.; Launois, P.; Van Tendeloo, G.; Lucas, A. A.; Lambin, P. Bundles of Identical Double-Walled Carbon Nanotubes. *Chem. Commun.* **2004**, 2592–2593.
14. Hashimoto, A.; Suenaga, K.; Urita, K.; Shimada, T.; Sugai, T.; Bandow, S.; Shinohara, H.; Iijima, S. Atomic Correlation Between Adjacent Graphene Layers in Double-Wall Carbon Nanotubes. *Phys. Rev. Lett.* **2005**, *94*, 045504.
15. Chandra, B.; Caldwell, R.; Huang, M.; Huang, L. M.; Sfeir, M. Y.; O'Brien, S. P.; Heinz, T. F.; Hone, J. Electrical Transport Measurements of Nanotubes with Known (*n*, *m*) Indices. *Phys. Status Solidi B* **2006**, *243*, 3359–3364.

16. Liu, K. H.; Wang, W. L.; Xu, Z.; Bai, X. D.; Wang, E. G.; Yao, Y. G.; Zhang, J.; Liu, Z. F. Chirality-Dependent Transport Properties of Double-Walled Nanotubes Measured *in Situ* on Their Field-Effect Transistors. *J. Am. Chem. Soc.* **2009**, *131*, 62–63.
17. Villalpando-Paez, F.; Son, H.; Nezich, D.; Hsieh, Y. P.; Kong, J.; Kim, Y. A.; Shimamoto, D.; Muramatsu, H.; Hayashi, T.; Endo, M.; *et al.* Raman Spectroscopy Study of Isolated Double-Walled Carbon Nanotubes with Different Metallic and Semiconducting Configurations. *Nano Lett.* **2008**, *8*, 3879–3886.
18. Bacsa, R. R.; Peigney, A.; Laurent, C.; Puech, P.; Bacsa, W. S. Chirality of Internal Metallic and Semiconducting Carbon Nanotubes. *Phys. Rev. B* **2002**, *65*, 161404(R).
19. Green, A. A.; Hersam, M. C. Properties and Application of Double-Walled Carbon Nanotubes Sorted by Outer-Wall Electronic Type. *ACS Nano* **2011**, *5*, 1459–1467.
20. Flahaut, E.; Bacsa, R.; Peigney, A.; Laurent, C. Gram-Scale CCVD Synthesis of Double-Walled Carbon Nanotubes. *Chem. Commun.* **2003**, 1442–1443.
21. Dyke, C. A.; Tour, J. M. Unbundled and Highly Functionalized Carbon Nanotubes from Aqueous Reactions. *Nano Lett.* **2003**, *3*, 1215–1218.
22. An, L.; Fu, Q.; Lu, C.; Liu, J. A Simple Chemical Route to Selectively Eliminate Metallic Carbon Nanotubes in Nanotube Network Devices. *J. Am. Chem. Soc.* **2004**, *126*, 10520–10521.
23. Bahr, J. L.; Tour, J. M. Highly Functionalized Carbon Nanotubes Using *in Situ* Generated Diazonium Compounds. *Chem. Mater.* **2001**, *13*, 3823–3824.
24. Cabana, J.; Martel, R. Probing the Reversibility of Sidewall Functionalization Using Carbon Nanotube Transistors. *J. Am. Chem. Soc.* **2007**, *129*, 2244–2245.
25. Iakoubovskii, K.; Minami, N.; Ueno, T.; Kazaoui, S.; Kataura, H. Optical Characterization of Double-Wall Carbon Nanotubes: Evidence for Inner Tube Shielding. *J. Phys. Chem. C* **2008**, *112*, 11194–11198.
26. Muramatsu, H.; Kim, Y. A.; Hayashi, T.; Endo, M.; Yonemoto, A.; Arikai, H.; Okino, F.; Touhara, H. Fluorination of Double-Walled Carbon Nanotubes. *Chem. Commun.* **2005**, 2002–2004.
27. Hayashi, T.; Shimamoto, D.; Kim, Y. A.; Muramatsu, H.; Okino, F.; Touhara, H.; Shimada, T.; Miyauchi, Y.; Maruyama, S.; Terrones, M.; *et al.* Selective Optical Property Modification of Double-Walled Carbon Nanotubes by Fluorination. *ACS Nano* **2008**, *2*, 485–488.
28. Dresselhaus, M. S.; Dresselhaus, G.; Saito, R.; Jorio, A. Raman Spectroscopy of Carbon Nanotubes. *Phys. Rep.* **2005**, *409*, 47–99.
29. Michel, T.; Paillet, M.; Nakabayashi, D.; Picher, M.; Jourdain, V.; Meyer, J. C.; Zahab, A. A.; Sauvajol, J.-L. Indexing of Individual Single-Walled Carbon Nanotubes from Raman Spectroscopy. *Phys. Rev. B* **2009**, *80*, 245416.
30. Wang, C.; Cao, Q.; Ozel, T.; Gaur, A.; Rogers, J. A.; Shim, M. Electronically Selective Chemical Functionalization of Carbon Nanotubes: Correlation Between Raman Spectral and Electrical Responses. *J. Am. Chem. Soc.* **2005**, *127*, 11460–11468.
31. Choi, H.; Ihm, J.; Louie, S.; Cohen, M. Defects, Quasibound States, and Quantum Conductance in Metallic Carbon Nanotubes. *Phys. Rev. Lett.* **2000**, *84*, 2917–2920.
32. Brozena, A. H.; Moskowitz, J.; Shao, B.; Deng, S.; Liao, H.; Gaskell, K. J.; Wang, Y. H. Outer Wall Selectively Oxidized, Water-Soluble Double-Walled Carbon Nanotubes. *J. Am. Chem. Soc.* **2010**, *132*, 3932–3938.
33. Yao, Z.; Kane, C. L.; Dekker, C. High-Field Electrical Transport in Single-Wall Carbon Nanotubes. *Phys. Rev. Lett.* **2000**, *84*, 2941–2944.
34. Park, J.-Y.; Rosenblatt, S.; Yaish, Y.; Sazonova, V.; Ustunel, H.; Braig, S.; Arias, T. A.; Brouwer, P. W.; McEuen, P. L. Electron-Phonon Scattering in Metallic Single-Walled Carbon Nanotubes. *Nano Lett.* **2004**, *4*, 517–520.
35. Javey, A.; Guo, J.; Paulsson, M.; Wang, Q.; Mann, D.; Lundstrom, M.; Dai, H. J. High-Field Quasiballistic Transport in Short Carbon Nanotubes. *Phys. Rev. Lett.* **2004**, 92.
36. Bourlon, B.; Glattli, D. C.; Placais, B.; Berroir, J. M.; Miko, C.; Forro, L.; Bachtold, A. Geometrical Dependence of High-Bias Current in Multiwalled Carbon Nanotubes. *Phys. Rev. Lett.* **2004**, 92.
37. Lazzeri, M.; Piscanec, S.; Mauri, F.; Ferrari, A.; Robertson, J. Electron Transport and Hot Phonons in Carbon Nanotubes. *Phys. Rev. Lett.* **2005**, *95*, 1–4.
38. Cabana, J.; Lavoie, S.; Martel, R. Thermal Chemistry of Methylene- and Phenyl-Functionalized Carbon Nanotubes. *J. Am. Chem. Soc.* **2010**, *132*, 1389–1394.
39. Aguirre-Carmona, C. M. Carbon Nanotube Networks for Thin Film Electronic Applications. Ph.D. Thesis, École Polytechnique de Montréal, 2007.
40. Kingston, C. T.; Jakubek, Z. J.; Dénommée, S.; Simard, B. Efficient Laser Synthesis of Single-Walled Carbon Nanotubes Through Laser Heating of the Condensing Vaporization Plume. *Carbon* **2004**, *42*, 1657–1664.
41. Choi, K.; Bourgoin, J.; Auvray, S.; Esteve, D.; Duesberg, G.; Roth, S.; Burghard, M. Controlled Deposition of Carbon Nanotubes on a Patterned Substrate. *Surf. Sci.* **2000**, *462*, 195–202.
42. Paillet, M.; Meunier, F.; Verhaegen, M.; Blais-Ouellette, S.; Martel, R. High Performance Resonance Raman Spectroscopy Using Volume Bragg Gratings as Tunable Light Filters. *Rev. Sci. Instrum.* **2010**, *81*, 053111.